Measurement of nonlinear refractive indices of bulk and liquid crystals by nonlinear chirped interferometry

Benjamin Maingot, Elizaveta Neradovskaia, Cyrille Claudet, Nicolas Forget, Aurélie Jullien

Measurement of the nonlinear refractive indices of bulk and liquid crystals by nonlinear chirped interferometry

Benjamin Maingot,[1,2] Elizaveta Neradovskaia,[1] Cyrille Claudet,[1] Nicolas Forget,[1,*] and Aurélie Jullien[1]

[1] *Université Côte d'Azur, CNRS, Institut de Physique de Nice (INPHYNI), UMR 7010, 17 rue Julien Lauprêtre, 06200 Nice, France*

[2] *Fastlite, 165 route des Cistes, 06600 Antibes, France*

The nonlinear refractive index (n_2) of a selection of bulk (LBO, KTA, MgO:$LiNbO_3$, LGS, ZnSe) and liquid (E7, MLC2132) crystals is measured at 1030 nm in the sub-picosecond regime (200 fs) by nonlinear chirped interferometry. The reported values provide key parameters for the design of near- to mid-infrared parametric sources as well as all-optical delay lines.

The third-order susceptibility tensor $\chi^{(3)}$ governs four-wave mixing processes [1]. The real part of the tensor is responsible for the optical Kerr effect (OKE) but also self-phase modulation (SPM), cross-phase modulation (XPM) and cross-polarized wave generation (XPW [2]). These frequency-degenerated non resonant nonlinear processes play fundamental roles in ultrafast optics as the propagation of short and intense pulses in dispersive $\chi^{(3)}$ media may lead to significant spectral broadening [3], spectral narrowing [4], distortion [5] and, possibly, filamentation and pulse/beam breakdown [6]. The magnitude of these effects may be assessed by computing the accumulated nonlinear phase shift along the beam propagation (B-integral), provided that the coefficients of the $\chi^{(3)}$ tensor of the different optical elements are known. It is thus essential to determine these coefficients for the materials where the peak intensity is the highest.

In this paper, we focus on some of the key components of optical parametric (chirped-pulse) amplifiers (OP(CP)A) pumped at 1.03 m. These systems, which have become the backbone of third-generation femtosecond sources [7], operate typically in the near- to mid-infrared and provide ultrashort pulses at high repetition rate - two key properties for vibrational spectroscopy [8] but also time-resolved ARPES [9]. Mid-infrared OPAs rely on nonlinear crystals featuring low absorption at the generated wavelengths, low two- and three-photon absorption at 1.03 μm as well as high damage threshold and good thermal conductivity [10–12]. Among the most widely used nonlinear OPA crystals are LiB_3O_5 (LBO), $KTiOAsO_4$ (KTA) and MgO:$LiNbO_3$ (MLN). We also include in this study $LiGaS_2$ (LGS), ZnSe, two liquid crystals (E7 and MLC2132) and Al_2O_3 as a reference medium. LGS has attracted great interest thanks to its extended transparency (up to 9-10 μm) and phase-matching properties compatible with a direct frequency-difference generation up to the thermal infrared [13, 14]. ZnSe is widely used for infrared components, due to its remarkably wide transmission in the infrared. E7 and MLC2132 are two liquid crystals (LCs) which found recent applications in the infrared, both as all-optical delay lines and as spatial light modulators [15–17]. All measurements are performed at 1.03 μm and in the short-pulse regime ($\simeq$200 fs).

To characterize the $\chi^{(3)}$ tensor elements, we exploit a method coined as "nonlinear chirped interferometry" [18], which is essentially a spectrally-resolved interferometric pump-probe experiment. The observable is the variation of the optical group delay of a transmitted probe with respect to a reference pulse, under the effect of a strong pump pulse. When the three pulses are adequately chirped, the probe-reference delay evolves with the pump-probe delay and scales with the nonlinearity of the propagation medium. This effect originates from two different mechanisms, coherently added up: (i) two-beam-coupling triggers energy exchanges between the chirped pump and probe pulses and induces temporal reshaping; (ii) the frequency-shift undergone by the probe via cross-phase modulation is encoded in time via the chirp of the reference pulse. Among the major advantages of this approach are the low sensitivity of the observable to the phase fluctuations of the interferometer, and the sensitivity enhancement provided by the use of chirped pulses. Nonlinear phase shifts as low as a few mrad can thus be detected without resorting to heterodyne detection and/or active stabilization [18].

The experimental setup is represented in Fig. 1. A Pharos laser system (PH1-SP-1mJ, Light Conversion) delivers 180 fs pulses, with a central wavelength of 1034 nm, a repetition rate of 1 kHz or 10 kHz, and a pulse energy up to 500 J. The beam is split into three separated beams: pump, probe and reference, the latter being selected before the nonlinear stage. The pump and probe beams are focused (f = 1.5 m) to about 550 μm FWHM and overlap in the sample under a small angle ($< 1°$). The maximum pump pulse peak intensity is around 100 GW/cm^2. The samples are thin enough to neglect diffraction, geometrical/birefringent walk-off as well as dispersion and group velocity mismatch in the interaction length. After the interaction, the probe is selected and recombined with the reference beam. The nominal group delay between the reference and the probe pulses (τ^0_{RPr}) is set to 3.5 ps for all measurements. The resulting interference pattern is collected by a spectrometer (Avantes, spectral resolution 0.07 nm) as a function of pump-probe delay

* Nicolas.Forget@inphyni.cnrs.fr

(τ_{PPr}). Since the pump beam is not spatially uniform, the interferogram is actually averaged over the pump-probe overlap area in the slit direction. As described in our former publication [18], chirping of the pulses adequately is required. The grating compressor of the laser system is detuned such that the output pulses are chirped to $\simeq$+5000 fs^2. A 20-mm SF11 rod ($\simeq$+2000 fs^2 at 1030 nm) is added to the reference beam path to improve the signal-to-noise ratio of the measurement [18]. The polarization direction and the pulse energy of all three beams are controlled by half-wave plates and thin-films polarizers (TFPs). The different components of the $\chi^{(3)}$ tensor of the sample are measured by varying the polarization direction of the three pulses, as summarized in Tab. I. Fig. 2 illustrates a typical experimental acquisition (MLC2132 LC sample). Fig. 2a features the acquired (single-shot) spectra as a function of the pump-probe delay. The frequency-shift shift induced by XPM is clearly visible in the vicinity of the pump-probe temporal overlap. A close-up of the Fourier transform near +3.5 ps is shown in Fig. 2b. The transient shift of the peak position of the Fourier transform is plotted in Fig. 2c. This curves displays a typical Z-shape, characterized by a delay swing and a slope between the two delay extrema. As demonstrated in [18], these two quantities (swing and slope) vary linearly with the nonlinear phase accumulated in the sample for phase excursions up to a few hundreds of mrad. The values of the involved tensor term(s) are then assessed by comparison/calibration with a well-characterized reference medium (here a 1-mm sapphire plate or a 1-mm silica plate). This calibration step not only dispenses with calculating the true peak intensity on the sample but also takes into account the spatial distribution of the pump beam intensity. In addition, since this Z-shape arises from the derivative of the nonlinear phase, an integration yields the third-order correlation of the pump pulse and provides an *in situ* estimate/check of the pulse duration in the sample (Fig. 2d). Here, the correlation width of $\simeq$280 fs FWHM is measured, which fits to a pulse duration of about 200 fs FWHM, as expected.

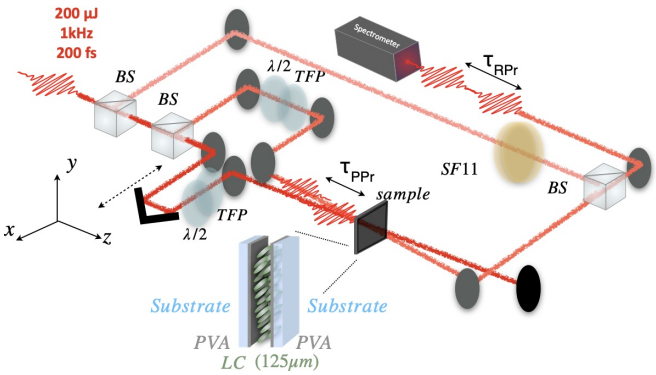

FIG. 1: Experimental setup. The laser source (Pharos SP, Light Conversion) is split into three beams (pump, probe, and reference). BS: beam splitter. TFP: thin film polarizer. $\lambda/2$: half-wave plates. The nonlinear sample is positioned on a 3-axis translation stage. Illustration of a LC sample.

TABLE I: Polarization configurations and measured components of $\chi^{(3)}$ tensor. x refers to the extraordinary axis (for a birefringent medium).

Pol. config.	Pump	Probe	Ref.	$\chi^{(3)}$ term
(i)	⇔	⇔	⇔	$\chi^{(3)}_{xxxx}$
(ii)	⇕	⇕	⇕	$\chi^{(3)}_{yyyy}$
(iii)	⇔	⇕	⇕	$\chi^{(3)}_{xxyy} + \chi^{(3)}_{xyxy}$
(iv)	⇕	⇔	⇔	$\chi^{(3)}_{yyxx} + \chi^{(3)}_{yxyx}$

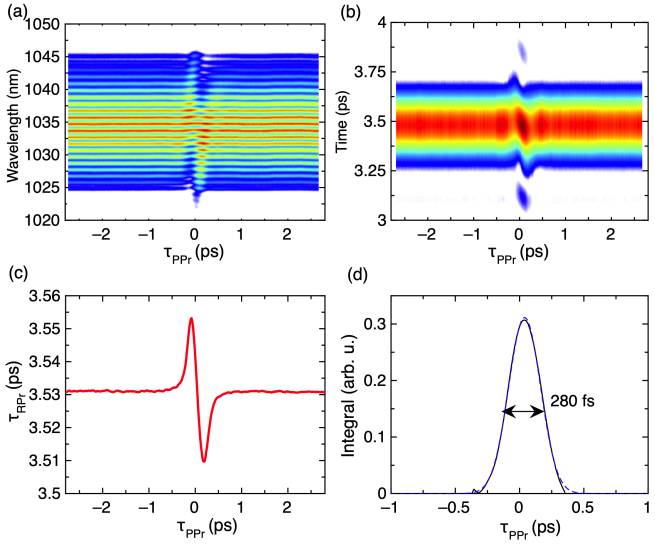

FIG. 2: Typical single-shot experimental data (LC sample). The nonlinear phase-shift accumulated by the probe is estimated to 500 mrad. (a) Interferogram of the probe and reference pulses as a function of pump-probe delay. (b) Sideband peak of the Fourier transform of the interferograms. (c) Position of the sideband peak (τ_{RPr}, i.e. optical group delay between reference and probe pulses, as a function of the pump-probe delay (τ_{PPr}). (d) Correlation profile of the pump pulse obtained from integration of (c).

The method is first applied to determine the third-order nonlinear susceptibility of MLC2132 and E7 LC mixtures (Merck) in the nematic phase. The samples consist in home-made cells, where the LC is inserted between two 1-mm-thick uncoated fused silica substrates. A thin film of polyvinyl alcohol (PVA) is spin-coated on the substrate and then rubbed to anchor and align the molecules in a plane parallel to the substrate. The thickness of the LC layer is assessed by spectral interferometry and found to be $126\mu m \pm 2\mu m$ for MLC2132 and $125\mu m \pm 2\mu m$ for E7 samples respectively [19–21]. An empty cell is also manufactured to discriminate the relative contribution of the substrates only and the LC layer.

For this experiment, the laser peak intensity is adjusted to 70 G W/cm^2, below the laser-induced damage threshold of the LC [22]. Third-harmonic generation is visible from the LC-substrate interfaces [23].

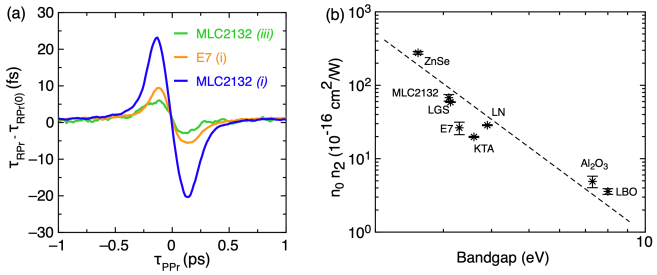

FIG. 3: (a) Relative optical group delay between reference and probe pulses (τ_{RPr}) as a function of pump-probe delay (τ_{PPr}), for MLC2132 and E7, configuration (i) and MLC2132 configuration (iii). (b) Nonlinear index dependence versus bandgap for the tested samples in log-log scale. The dashed line indicates a E_g^{-4} dependence.

Some experimental results, for the two liquid crystals, are presented in Fig. 3a. With polarization configuration (i) the retrieved extraordinary nonlinear index of MLC2132 and E7 is, respectively, $(3.87 \pm 0.4) \times 10^{-15}$ cm^2/W and $(1.55 \pm 0.3) \times 10^{-15}$ cm^2/W. In polarization configuration (ii), which corresponds to the ordinary index, the measurement yields $(4.4 \pm 0.4) \times 10^{-16}$ cm^2/W and $(2.44 \pm 0.3) \times 10^{-15}$ cm^2/W. Tab. III summarizes the experimental results for various polarization configurations. With the same experimental setup we characterized samples of lithium triborate (LiB_3O_5, LBO), potassium titanyl arsenate ($KTiOAsO_4$, KTA), magnesium doped congruent lithium niobate (5% MgO:$LiNbO_3$, MLN) and lithium gallium sulfide ($LiGaS_2$,LGS). The thickness and crystallographic orientations of the samples are reported in Tab. IV. For KTA, MLN and LGS the orientation corresponds to type-I phase matching condition for a pump wavelength at 1030 nm and idler wavelengths lying in the 2-10 m range. The nonlinear index is measured along the slow and fast axis, except for LBO. A ZnSe crystal is also characterized to cross-check the measurement protocol. The pump energy is adapted for each sample, so as to keep the nonlinear phase within the linearity range of the detection method (i.e. below 500 mrad). The results are reported in Tab. IV. We emphasize the high reproducibility of our measurements, which translates into lower estimated errors than traditional methods (Z-scan, mostly).

We note that the nonlinear index of LGS is twice higher than MLN, itself higher than KTA. We underline the large nonlinear properties of ZnSe, with a nonlinear index nearly two orders of magnitude higher than sapphire, as also noticed in [29]. The measured values are in quite good agreement for LBO, MLN and ZnSe with the data found in the literature at 1030 nm. We stress that the

TABLE II: Linear refractive index values from [21] and measured nonlinear index values ($\times 10^{-16}$ cm^2/W) for nematic E7 and MLC2132, for λ= 1030 nm. The reference sample is fused silica.

LC sample	n^e	n^o	n_2^e	n_2^o
E7	1.70	1.51	15.5 ± 0.3	2.44 ± 0.3
MLC2132	1.72	1.49	38.7 ± 0.4	4.4 ± 0.4

TABLE III: Measured values of some of the terms of the $\chi^{(3)}$ tensor for the MLC2132 and E7 mixtures. The values are relative to that of fused silica ($\chi_0 = (2.0 \pm 0.2)\, 10^{-22}\, \mathrm{m}^2/\mathrm{V}^2$ [24]). x refers to the extraordinary axis of the LC cells. The last column gathers the calculated experimental nonlinear phase in the LC layer.

Mixture	$\chi^{(3)}$ term	$\chi^{(3)}$ value	φ_{NL} (mrad)
MLC2132	$\chi^{(3)}_{xxxx}$	$(17 \pm 3) \times \chi_0$	105
	$\chi^{(3)}_{yyyy}$	$(3.5 \pm 0.5) \times \chi_0$	20
	$\chi^{(3)}_{xxyy} + \chi^{(3)}_{xyxy}$	$(1.3 \pm 0.2) \times \chi_0$	9
	$\chi^{(3)}_{yyxx} + \chi^{(3)}_{yxyx}$	$(2.8 \pm 0.5) \times \chi_0$	18
E7	$\chi^{(3)}_{xxxx}$	$(7.1 \pm 1) \times \chi_0$	40
	$\chi^{(3)}_{yyyy}$	$(1.08 \pm 0.1) \times \chi_0$	5
	$\chi^{(3)}_{xxyy} + \chi^{(3)}_{xyxy}$	$(4.4 \pm 0.8) \times \chi_0$	15
	$\chi^{(3)}_{yyxx} + \chi^{(3)}_{yxyx}$	$(3.8 \pm 0.7) \times \chi_0$	12

TABLE IV: Measured nonlinear refractive indices of LBO, KTA, MLN, LGS and ZnSe at 1030 nm for 200 fs pulses. For birefringent crystals, values are given for the fast axis (low index, lo) and/or for the slow axis (high index, hi). θ and ϕ refers to the polar crystallographic orientation. L is the crystal length. All values from literature were measured near 1030 nm with sub-ps pulses, with the exception of MgO:LN and LBO, for which the reported values at 800 nm were rescaled (*) to 1030 nm as described by [25] and references). The reference sample is sapphire.

Sample	θ °	ϕ °	L mm	$n_{2,\mathrm{meas}}$ 10^{-20} m^2/W	$n_{2,\mathrm{lit}}$
Al_2O_3	0	-	1	-	2.8 ± 0.5 [26]
LBO lo	90	10	2.3	2.24 ± 0.2	
	90	-	5		2.2 ± 0.25* [27]
KTA lo	41.8	0	1.5	10.6 ± 0.2	
	42	0	4		15 [28]
KTA hi	41.8	0	1.5	11.2 ± 0.2	
	42	0	4		15 [28]
MLN lo	45.4	30	2	12.6 ± 0.2	
MLN hi	45.4	30	2	14.3 ± 0.4	
	0	-	2		16.7 ± 2.5* [27]
LGS lo	47	0	1	28.1 ± 0.3	
	48.2	0	5		41 [28]
	90	38.8	7		35 [10]
	90	37.5	2		¡ 64 [11]
LGS hi	47	0	1	31 ± 0.3	
	48.2	0	5		41 [28]
ZnSe	-	-	2	112 ± 1.6	113 ± 12 [29]

reported n_2 values aggregate different sources of nonlinearities: instantaneous electronic response, delayed Raman response, cascaded quadratic effects. As detailed in [25, 30], the relative contributions of these source terms to the total nonlinearity may vary significantly with both pulse duration and wavelength. Therefore, the discrepancies with regards to the literature may originate from differences in crystallographic orientation and/or pulse duration and/or wavelength. KTA, in particular, exhibits a strong Raman ringing at our pulse duration [18], which is expected to decrease the total nonlinearity.

For LCs, the Kerr-like nonlinearity of LCs was previously established as orders of magnitude higher than in bulk material [31], due to complex nonlocal molecular dynamics such as laser-induced director axis reorientation, thermal or order parameter fluctuations, and even photorefractivity [32]. Despite the growing interest of LCs for ultrashort pulse manipulation, especially in the near- and mid-infrared spectral ranges [15–17], only a few studies report on the use of LCs for ultrafast nonlinear optics [33–36] or for ultra-intense laser-matter interaction [37]. Z-scan measurements in dye-doped LCs [38] or isotropic LCs with strong two-photon absorption [31] have estimated the electronic nonlinear index of these mixtures to about $10^{-15}\text{cm}^2/\text{W}$. In Fig.3b is plotted the measured nonlinear index versus the bandgap energy (E_g) of the tested samples. As expected for bulk dielectrics complying to a two-band model [39], the trend follows a E_g^{-4} law. The measured nonlinear index of MLC2132 fits within this picture, considering a linear index of 1.72 [21] and an energy bandgap of $\simeq$3.1 eV [40]. Interestingly, these results indicate that the nonlinear index of the E7 and MLC2132 LCs could be adjusted over almost an order of magnitude but applying a voltage to control the orientation the molecular director.

To conclude, we measured by nonlinear chirped interferometry the (previously unknown) nonlinear indices of the E7 and MLC2132 nematic mixtures at 1030 nm in the sub-ps regime. We also measured, by the same means and in the same conditions, the nonlinear indices of KTA, MLN and LGS along the crystallographic orientations of interest for type-I difference frequency generation (or, equivalently, optical parametric amplification) with a 1030 nm pump. We believe that these values will provides crucial design parameters for high-average-power mid-infrared OPCPA sources based on Ytterbium pump lasers.

FUNDING

We acknowledge financial support from the Agence Nationale de la Recherche France (Grant ANR-19-CE30-0006-01 UNLOC), the European Regional Development Fund (OPTIMAL) and from the European Unions Horizon 2020 research and innovation program under the Marie Skodowska-Curie grant agreement No 860553.

DISCLOSURES

The authors declare no conflicts of interest.

DATA AVAILABILITY STATEMENT

Data underlying the results presented in this paper are not publicly available at this time but may be obtained from the authors upon reasonable request.

[1] R. L. Sutherland, *Handbook of nonlinear optics* (Marcel Dekker INC, 2003).
[2] A. Jullien, O. Albert, G. Chériaux, J. Etchepare, S. Kourtev, N. Minkovski, and S. M. Saltiel, J. Opt. Soc. Am. B **22**, 2635 (2005).
[3] G. P. Agrawal, in *Nonlinear Science at the Dawn of the 21st Century* (Springer, 2000) pp. 195–211.
[4] M. Oberthaler and R. Höpfel, Applied Physics Letters **63**, 1017 (1993).
[5] R. Zhang, D. Pang, and Q. Wang, Appl. Opt. **41**, 1108 (2002).
[6] R. R. Alfano and S. Shapiro, Physical Review Letters **24**, 592 (1970).
[7] H. Fattahi, H. G. Barros, M. Gorjan, T. Nubbemeyer, B. Alsaif, C. Y. Teisset, M. Schultze, S. Prinz, M. Haefner, M. Ueffing, *et al.*, Optica **1**, 45 (2014).
[8] J. D. Pickering, M. Bregnhoj, A. S. Chatterley, M. H. Rasmussen, S. J. Roeters, K. Strunge, and T. Weidner, Biointerphases **17**, 011202 (2022).
[9] A. Grubisic Cabo, J. A. Miwa, S. S. Grønborg, J. M. Riley, J. C. Johannsen, C. Cacho, O. Alexander, R. T. Chapman, E. Springate, M. Grioni, *et al.*, Nano letters **15**, 5883 (2015).
[10] M. Seidel, X. Xiao, S. A. Hussain, G. Arisholm, A. Hartung, K. T. Zawilski, P. G. Schunemann, F. Habel, M. Trubetskov, V. Pervak, O. Pronin, and F. Krausz, Science Advances **4**, eaaq1526 (2018).
[11] M. Namboodiri, C. Luo, G. Indorf, T. Golz, I. Grguraš, J. H. Buss, M. Schulz, R. Riedel, M. J. Prandolini, and T. Laarmann, Opt. Mater. Express **11**, 231 (2021).
[12] B.-H. Chen, E. Wittmann, Y. Morimoto, P. Baum, and E. Riedle, Opt. Express **27**, 21306 (2019).
[13] Z. Heiner, L. Wang, V. Petrov, and M. Mero, Opt. Express **27**, 15289 (2019).
[14] V. Femy, M. Neradovskiy, T. Pinoteau, J. Villanueva, O. Albert, and N. Forget, in *Frontiers in Optics + Laser Science 2021* (Optica Publishing Group, 2021) p. FTh4B.4.
[15] A. Jullien, U. Bortolozzo, S. Grabielle, J.-P. Huignard, N. Forget, and S. Residori, Opt. Express **24**, 14483 (2016).
[16] V. M. di Pietro, S. Bux, N. Forget, and A. Jullien, Opt. Lett. **45**, 543 (2020).
[17] M. Neradovskiy, A. Scarangella, A. Jullien, and M. Mitov, Opt. Express **27**, 21794 (2019).

[18] E. Neradovskaia, B. Maingot, G. Chériaux, C. Claudet, N. Forget, and A. Jullien, APL Photonics **7**, 116103 (2022).
[19] L. Lepetit, G. Chériaux, and M. Joffre, J. Opt. Soc. Am. B **12**, 2467 (1995).
[20] A. Borzsonyi, A. P. Kovács, and K. Osvay, Applied Sciences **3**, 515 (2013).
[21] V. M. D. Pietro and A. Jullien, Applied Sciences **10**, 4701 (2020).
[22] L. Ramousse, G. Chériaux, C. Claudet, and A. Jullien, Appl. Opt. **60**, 8050 (2021).
[23] D. Yelin, Y. Silberberg, Y. Barad, and J. S. Patel, Phys. Rev. Lett. **82**, 3046 (1999).
[24] U. Gobler and C. Bosshard, Phys. Rev. B **61**, 10702 (2000).
[25] M. Bache and R. Schiek, arXiv preprint arXiv:1211.1721 (2012).
[26] A. Major, F. Yoshino, I. Nikolakakos, J. S. Aitchison, B. Lavorel, and P. W. E. Smith, Opt. Lett. **29**, 602 (2004).
[27] H. P. Li, C. H. Kam, Y. L. Lam, and W. Ji, Optical Materials **15**, 237 (2001).
[28] M. Mero, L. Wang, W. Chen, N. Ye, G. Zhang, V. Petrov, and Z. Heiner, Pacific Rim Laser Damage 2019: Optical Materials for High-Power Lasers **11063**, 40 (2019).
[29] G. N. Patwardhan, J. S. Ginsberg, C. Y. Chen, M. M. Jadidi, and A. L. Gaeta, Opt. Lett. **46**, 1824 (2021).
[30] M. Bache, H. Guo, B. Zhou, and X. Zeng, Opt. Mater. Express **3**, 357 (2013).
[31] I. C. Khoo, S. Webster, S. Kubo, W. J. Youngblood, J. D. Liou, T. E. Mallouk, P. Lin, D. J. Hagan, and E. W. V. Stryland, Journal of Materials Chemistry **19**, 7525 (2009).
[32] I. C. Khoo, Progress in Quantum Electronics **38**, 77 (2014).
[33] L. Cattaneo, M. Savoini, I. Muševič, A. Kimel, and T. Rasing, Opt. Express **23**, 14010 (2015).
[34] C.-W. Chen, X. Guo, X. Ni, T.-H. Lin, and I. C. Khoo, Opt. Mater. Express **7**, 2005 (2017).
[35] Y. Liu, S. Fu, B. A. Malomed, I. C. Khoo, and J. Zhou, Applied Sciences **7**, 556 (2017).
[36] Y. Liu, H. Liang, C.-W. Chen, X. Xie, W. Hu, P. Chen, J. Wen, J. Zhou, T.-H. Lin, and I. C. Khoo, Opt. Express **26**, 28818 (2018).
[37] P. L. Poole, C. Willis, G. E. Cochran, R. T. Hanna, C. D. Andereck, and D. W. Schumacher, Appl. Phys. Lett. **109**, 151109 (2016).
[38] V. Gayvoronsky, S. Yakunin, V. Enikeeva, I. Ozheredov, and A. Shkurinov, Laser Phys. Lett. **3**, 357 (2006).
[39] M. Sheik-Bahae, D. Hutchings, D. Hagan, and E. V. Stryland, IEEE J. Quantum Electron. **27**, 1296 (1991).
[40] T. Z. Kosc, A. A. Kozlov, S. Papernov, K. R. P. Kafka, K. L. Marshall, and S. G. Demos, Scientific Reports **9**, 16435 (2019).

chi(3)